Coalescence of Anderson-localized modes at an exceptional point in 2D random media

Nicolas Bachelard, A. Schumer, B. Kumar, C. Garay, J. Arlandis, R. Touzani, P. Sebbah

Coalescence of Anderson-localized modes at an exceptional point in 2D random media

N. Bachelard,[1,2,3] A. Schumer,[3] B. Kumar, [5] C. Garay,[1] J. Arlandis,[1] R. Touzani,[4] and P. Sebbah[5,1,*]

[1] *Institut Langevin, ESPCI ParisTech, CNRS, 75238 Paris Cedex 05, France*
[2] *Université de Bordeaux, CNRS, LOMA, UMR 5798, 33405 Talence, France*
[3] *Institute for Theoretical Physics, Vienna University of Technology (TU Wien), 1040 Vienna, Austria*
[4] *Laboratoire de Mathématiques, Université Blaise Pascal, CNRS (UMR 6620), 63177 Aubière Cedex, France*
[5] *Department of Physics, The Jack and Pearl Resnick Institute for Advanced Technology, Bar-Ilan University, Ramat-Gan 5290002, Israel*
[*] *patrick.sebbah@biu.ac.il*

Abstract: In non-Hermitian settings, the particular position at which two eigenstates coalesce in the complex plane under a variation of a physical parameter is called an exceptional point. An open disordered system is a special class of non-Hermitian system, where the degree of scattering directly controls the confinement of the modes. Herein a non-perturbative theory is proposed which describes the evolution of modes when the permittivity distribution of a 2D open dielectric system is modified, thereby facilitating to steer individual eigenstates to such a non-Hermitian degeneracy. The method is used to predict the position of such an exceptional point between two Anderson-localized states in a disordered scattering medium. We observe that the accuracy of the prediction depends on the number of localized states accounted for. Such an exceptional point is experimentally accessible in practically relevant disordered photonic systems.

1. Introduction

Most physical systems are subject to inherent losses, either because of dissipation or openness, and are described mathematically by a non-Hermitian Hamiltonian. This generally implies that the eigenstates of the Hamiltonian are complex as well as non-orthogonal. In such systems, the interrelation between pairs of eigenstates under the variation of a set of external parameters is essentially dictated by the existence of exceptional points (EPs). At an EP not only eigenvalues but also eigenstates degenerate, i.e. eigenvectors have the same amplitudes and a constant phase shift. The eigenvalue surfaces display a singular topology in the presence of an EP [1] while the eigenstates accumulate a residual geometric phase upon encircling the EP in parameter space [2, 3]. Since their introduction by Kato in 1966 [4], EPs have been associated with numerous often counterintuitive physical effects [5–8] that include mode hybridization [9], quantum phase transitions [10], reversal of the pump dependence of a laser [11], Parity-Time (*PT*) symmetry breaking [12, 13], increased sensitivity to perturbations [14, 15] or spectrally broad coherent perfect absorption [16]. They have been observed experimentally in a variety of different systems such as microwave billiards [17], chaotic optical microcavities [18], optomechanical arrangements [19], Fabry-Pérot resonators [20], two level atoms in high-Q cavities [8], coupled photonic-crystals [21], coupled acoustic cavities [22], optical fibres [23] or electronic circuits [24]. Open random media constitute a special class of non-Hermitian systems. Here, modal confinement depends almost entirely on the degree of scattering. In the regime of strong scattering, modes can experience Anderson-localization—a multi-scattering interference phenomenon where the spatial extension of the modes becomes smaller than the system size resulting in transport inhibition [25]. These disorder-induced localized states, for example, provide a natural

optical cavity in random lasers [26–28] and showed to be good candidates for cavity quantum electrodynamics (QED) [29, 30], with the main advantage of being inherently disorder-robust. By locally tuning the disorder, e.g. by gradually adjusting the dielectric permittivity, these states can be engineered to spatially and spectrally overlap to form so-called necklace states [31–33], which represent open channels in a nominally localized system [34, 35]. The formation of necklace states is considered a key mechanism in the transition from localization to the diffusive regime [36]. While EPs and, in general, *PT*-symmetry have been studied in the context of disordered media [21, 28, 37–41], coalescing localized modes and their associated degeneracies have not been studied so far.

In this work, the coalescence of two Anderson-localized optical modes in a two-dimensional (2D) dielectric random system is invoked by manipulating the dielectric permittivity at two different locations in the system. We first propose a general analytical analysis to follow the spectral and spatial evolution of modes in 2D dielectric open media. Then, this approach is applied to the specific case of Anderson-localized modes to identify the position of an EP in the parameter space. The prediction is tested numerically with finite element method (FEM) simulations. Remarkably, in this open disordered system a conventional two-mode model, prominently used in a variety of EP-related studies, would fail badly. The modification of a few single scatterers affects a multitude of modes and eventually influences the position of the degeneracies. This emphasizes the complexity of eigenstate interactions in disordered media. We believe that our approach opens the way to a controlled local manipulation of the permittivity and the possibility to engineer hybridized and coupled localized modes. Furthermore, we think this approach can be easily extended to other kinds of resonant systems, e.g. coupled arrays of cavities [42, 43].

2. Theory and applications

2.1. Generalized eigenvalue problem

First, we consider the general case of a finite-size dielectric medium in 2D space with an inhomogeneous dielectric constant distribution $\epsilon(\mathbf{r})$. The speed of light is set to $c = 1$ such that frequencies are hence measured in multiples of c having a unit of m^{-1}. The electric field is assumed transverse and thus its polarization is neglected such that it satisfies the scalar Helmholtz equation

$$\Delta E(\mathbf{r},\omega) + \epsilon(\mathbf{r})\omega^2 E(\mathbf{r},\omega) = 0, \tag{1}$$

where $E(\mathbf{r},\omega)$ stands for the scalar electric field in the frequency domain. Eigensolutions of Eq. (1) define the modes or eigenstates of the problem

$$\Omega_i,\ |\Psi_i\rangle\ :\quad \Delta|\Psi_i\rangle + \epsilon(\mathbf{r})\Omega_i^2|\Psi_i\rangle = 0, \quad i \in \mathbb{N}, \tag{2}$$

where boundary conditions are fixed by Siegert-Gamow outgoing conditions. Because of its openness the system has inherent losses, thus described by a non-Hermitian Hamiltonian. In non-Hermitian systems modes are *a priori* non-orthogonal, complex and their completeness is not ensured. Here, we consider open systems with finite range permittivity $\epsilon(\mathbf{r})$ and where a discontinuity in the permittivity provides a natural demarcation of the problem. Under these two conditions Leung *et al.* [44–46] demonstrated the completeness of the set of eigenstates. The electric field can therefore be expanded in the basis of these modes as

$$E(\mathbf{r},\omega) = \sum_i a_i(\omega)|\Psi_i\rangle\,, \tag{3}$$

where the $a_i(\omega)$ are the complex expansion coefficients. For non-degenerate eigenstates a biorthogonal inner product [47, 48] can be defined via

$$\langle\Psi_p^*|\epsilon(\mathbf{r})|\Psi_q\rangle = \int_{\mathbb{R}^2} \epsilon(\mathbf{r})\Psi_p(\mathbf{r})\Psi_q(\mathbf{r})\mathrm{d}\mathbf{r} = \delta_{pq}. \tag{4}$$

Now, consider two locations $\mathbf{R}_1$ and $\mathbf{R}_2$ where the permittivity is varied

$$\tilde{\epsilon}(\mathbf{r}) = \epsilon(\mathbf{r}) + \Delta\epsilon_1 p_1(\mathbf{r}) + \Delta\epsilon_2 p_2(\mathbf{r}), \tag{5}$$

where $p_i(\mathbf{r}) = \delta(\mathbf{r} - \mathbf{R}_i)$ is the location and $\Delta\epsilon_i$ the amplitude of the permittivity variation. Equation (1) becomes

$$\left[\Delta + \omega^2(\epsilon(\mathbf{r}) + \Delta\epsilon_1 p_1(\mathbf{r}) + \Delta\epsilon_2 p_2(\mathbf{r}))\right] E(\mathbf{r}, \omega) = 0. \tag{6}$$

The permittivity distribution $\tilde{\epsilon}(\mathbf{r})$ describes a new disordered system associated with a new set of eigenstates $(\tilde{\Omega}_i, |\tilde{\Psi}_i\rangle)_{i\in\mathbb{N}}$. The electric field of the modified system written in terms of the basis of the original random system reads

$$E(\mathbf{r}, \omega) = \sum_i b_i(\omega)|\Psi_i\rangle, \tag{7}$$

where $b_i(\omega)$ are the new expansion coefficients. Inserting Eq. (7) into Eq. (6) gives

$$\sum_i b_i(\omega)\left[\Delta + \omega^2\left(\epsilon(\mathbf{r}) + \Delta\epsilon_1 p_1(\mathbf{r}) + \Delta\epsilon_2 p_2(\mathbf{r})\right)\right]|\Psi_i\rangle = 0. \tag{8}$$

Projecting $\langle\Psi_j^*|$ onto Eq. (8) using Eq. (2) and the biorthogonal product in Eq. (4) leads to

$$b_i(\omega)\left(\Omega_i^2 - \omega^2\right) = \omega^2 \sum_j C_{ij} b_j(\omega) \quad \forall i, \tag{9}$$

where

$$C_{ij} = \langle\Psi_i^*|\Delta\epsilon_1 p_1(\mathbf{r})|\Psi_j\rangle + \langle\Psi_i^*|\Delta\epsilon_2 p_2(\mathbf{r})|\Psi_j\rangle. \tag{10}$$

If we consider a finite set of N modes, Eq. (9) can be written conveniently in the form of a generalized eigenvalue problem

$$\left[\begin{pmatrix} \Omega_1^2 & \dots & 0 \\ \vdots & \ddots & \vdots \\ 0 & \dots & \Omega_N^2 \end{pmatrix} - \omega^2 \begin{pmatrix} 1 + C_{11} & \dots & C_{1N} \\ \vdots & \ddots & \vdots \\ C_{N1} & \dots & 1 + C_{NN} \end{pmatrix}\right] \begin{pmatrix} b_1(\omega) \\ \vdots \\ b_N(\omega) \end{pmatrix} = 0, \tag{11}$$

where the eigensystem of the perturbed setting is given via $\tilde{\Omega}_i^2 = \omega_i^2$ and $|\tilde{\Psi}_i\rangle = \sum_j b_j(\tilde{\Omega}_i)|\Psi_j\rangle$, which are the eigensolutions of Eq. (1) for the permittivity distribution $\tilde{\epsilon}(\mathbf{r})$. In Eq. (11), the coupling coefficients, C_{ij}, between original modes i and j depend on the variation of the permittivity and the spatial overlap of the modes at the location of the permittivity modification. Interestingly, the coupling integral not only depends on the spatial overlap of the mode intensity profiles, but also on the overlap of their spectral distributions. Remarkably, when reduced to two modes, the system is the analog of two inductance/capacitor oscillators coupled via an inductance L_c, in which charges of both capacitors satisfy

$$\begin{pmatrix} \left(\frac{1}{\sqrt{L_1 C_1}}\right)^2 & 0 \\ 0 & \left(\frac{1}{\sqrt{L_2 C_2}}\right)^2 \end{pmatrix} - \omega^2 \begin{pmatrix} 1 + \frac{L_C}{L_1} & \frac{L_c}{L_1} \\ \frac{L_c}{L_2} & 1 + \frac{L_c}{L_2} \end{pmatrix} = 0. \tag{12}$$

Equation (11) extends this result to any number of interacting modes $N > 2$ essentially describing a network of linearly coupled oscillators.

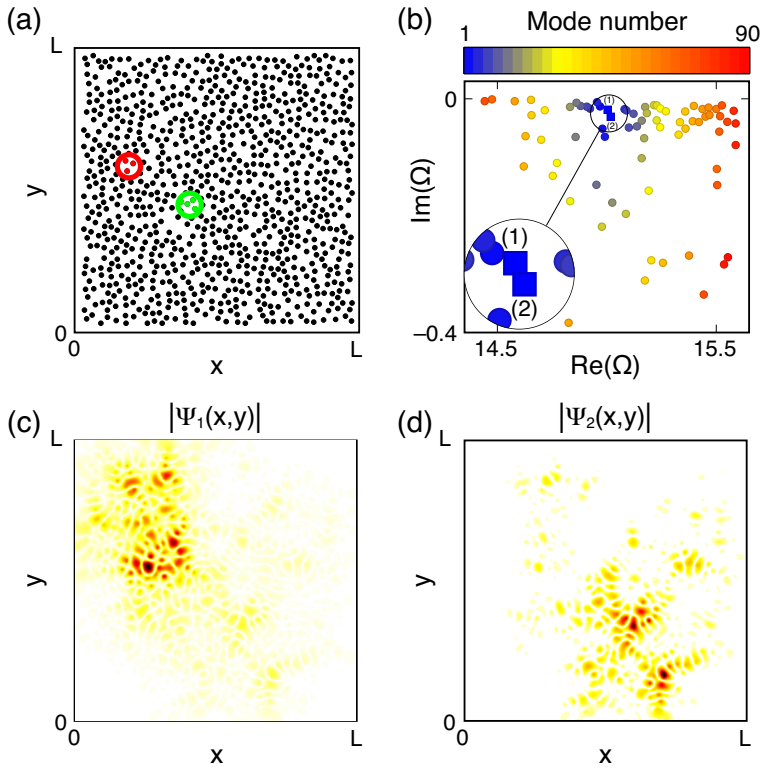

Fig. 1. (a) 2D random medium: 896 scatterers with dielectric permittivity $\epsilon = 4$ are embedded in vacuum $\epsilon_{\text{mat}} = 1$. The system is open at its boundaries. The permittivity is modified in the two colored regions, red and green circles, centered at positions $\mathbf{R}_1$ and $\mathbf{R}_2$, respectively. (b) Unperturbed eigenvalues $\Omega_i, i \in 1, \ldots, 90$, computed by FEM and sorted in the complex plane according to the distance $d(1, i)$ (see text). The insert points out eigenvalues of interest (namely Ω_1 and Ω_2). (c) and (d) Spatial distribution of the absolute value of the amplitude for the eigenvectors $|\Psi_1\rangle$ and $|\Psi_2\rangle$, respectively.

2.2. Identifying an EP between two Anderson-localized states

The formalism presented above is now applied to a 2D random collection of 896 circular dielectric scatterers (radius 60 nm) with dielectric permittivity $\epsilon = 4$ embedded in a host material of index $\epsilon_{\text{mat}} = 1$, with a filling fraction of 40% [Fig. 1(a)]. The system dimensions are $L \times L = 5.3 \times 5.3\,\mu\text{m}^2$. The interference effects, originating from multiple scattering leads to spatial confinement by the disorder known as Anderson localization and characterized by a localization length ξ. In the spectral range considered in the following, ξ is estimated to be around $1\mu\text{m} \ll L$ and thus the energy of the modes is mostly confined in the system: The modes are localized. The two circular regions with 340 nm diameter centered at $\mathbf{R}_1$ and $\mathbf{R}_2$ are shown in Fig. 1(a) as red and green circles, respectively. Within these regions the dielectric permittivity of the scatterers is varied from ϵ to $\epsilon + \Delta\epsilon_1$ and $\epsilon + \Delta\epsilon_2$, respectively.

The initial modes $(\Omega_i, |\Psi_i\rangle)$, $i \in 1, \ldots, N$, which are the only input requested by Eq. (11), are computed using FEM simulation [49, 50] with absorbing boundary conditions that are placed $0.4\,\mu\text{m}$ away from each side of the system. A large number of modes ($N = 90$) are computed for the initial system [Fig. 1(b)] in a narrow spectral range and we check that none of them are degenerate. Two localized states $|\Psi_1\rangle$ and $|\Psi_2\rangle$, corresponding to Ω_1 and Ω_2 respectively, are selected for being spectrally close [Fig. 1(b)] but spatially distinct [Fig. 1(c),(d)]. The spectral

distance between mode i and mode 1 is defined as $d(1,i) = |\Omega_1 - \Omega_i|$ and is visualized in the color-coding of Fig. 1(b). Here, mode 2 has the largest spectral overlap with mode 1 but we will see that the influence of other nearby modes cannot be neglected in the modal interaction. The initial modes obtained via a FEM are spatially defined in a finite spatial domain V while the biorthogonal product of Eq. (4) is an integral over all $\mathbb{R}^2$. However, it can be split into an integral over V and a second term at the boundary of V which replaces outside propagation [51]. Because the modes are localized their amplitudes along the boundary of V are very small. Neglecting the edge term in the biorthogonal product leads to an inaccuracy of around 0.8% in the ensuing calculation of the EP position. Boundary terms can therefore be safely neglected in the biorthogonal product.

Now, the permittivity distribution $\epsilon(\mathbf{r})$ is altered by $(\Delta\epsilon_1, \Delta\epsilon_2)$ and the corresponding eigensystem is calculated from Eq. (11) for $N = 60$ interacting modes for each pair $(\Delta\epsilon_1, \Delta\epsilon_2)$ in this two-dimensional parameter space, from which a new set of modes $(\tilde{\Omega}_i, |\tilde{\Psi}_i\rangle)$ is obtained. The spectral distance $\tilde{d}(1,2) = |\tilde{\Omega}_1 - \tilde{\Omega}_2|$ is shown in Fig. 2(a) for all values of the pair $(\Delta\epsilon_1, \Delta\epsilon_2)$. The sharp drop of $\tilde{d}(1,2)$ to zero observed at $(\Delta\epsilon_1, \Delta\epsilon_2)_{\mathrm{EP}} = (0.939, 0.90)$ reveals the existence of an EP, where both eigenvalues become degenerate. The evolution in the parameter space of the real and imaginary part of the eigenvalues, $\tilde{\Omega}_1$ and $\tilde{\Omega}_2$, is represented separately in Fig. 2(c),(d). The intricate topology of self-intersecting Riemann sheets at precisely the position $(\Delta\epsilon_1, \Delta\epsilon_2)_{\mathrm{EP}}$, corroborates the existence of an EP, where both the real and imaginary part of the eigenvalues cross. At this singular position, the corresponding eigenfunctions become collinear. This is demonstrated in Fig. 2(b), where the function $(1 - |\langle\tilde{\Psi}_1|\tilde{\Psi}_2\rangle|)^{-1}$ is found to diverge.

2.3. Testing the theoretical prediction

To substantiate the analytical prediction, the first two eigenvectors $(|\tilde{\Psi}_1\rangle, |\tilde{\Psi}_2\rangle)$ of the modified permittivity distribution $\tilde{\epsilon}(\mathbf{r})$ are calculated via numerical FEM simulations for each point $(\Delta\epsilon_1, \Delta\epsilon_2)$ on a grid in a range that encloses $(\Delta\epsilon_1, \Delta\epsilon_2)_{\mathrm{EP}}$. The sampling is set to 0.04 along the two parameters $\Delta\epsilon_1$ and $\Delta\epsilon_2$. The numerically computed eigenvalues merge at $(\Delta\epsilon_1, \Delta\epsilon_2) = (0.92, 0.88) \pm (0.04, 0.04)$, such that the predicted value from Eq. (11) is within the error bars. The collinearity of the eigenvectors is also numerically confirmed (not shown). Finally, the coalescing mechanism of modes 1 and 2 is described in Fig. 2(e) where modes with identical real (imaginary) parts are plotted in the parameter space, $(\Delta\epsilon_1, \Delta\epsilon_2)$, as blue (red) dots. At the EP where real and imaginary parts are equal simultaneously, the red and blue trajectories meet. Near this position, we compute the real (imaginary) part of the two eigenvectors, $\tilde{\Psi}_1(x, y)$ and $\tilde{\Psi}_2(x, y)$. Their distribution is shown in the insets of Fig. 2(e)]. Starting from the unperturbed modes $\Psi_1(x, y)$ and $\Psi_2(x, y)$ [shown in Fig. 1(c),(d)], both eigenvectors are progressively modified when approaching the EP. In the vicinity of the EP, $\mathrm{Re}(\tilde{\Psi}_1)$ converges to $\mathrm{Im}(\tilde{\Psi}_2)$ and $\mathrm{Im}(\tilde{\Psi}_1)$ to $-\mathrm{Re}(\tilde{\Psi}_2)$. Therefore, the eigenvectors display the same amplitude and a phase shift of $\pi/2$, $\tilde{\Psi}_1 = -i\tilde{\Psi}_2$, i.e. they become collinear at the EP. The amplitude of the degenerate eigenstate at the EP, $|\tilde{\Psi}_{\mathrm{EP}(1,2)}\rangle$, is shown in the inset of Fig. 3(a). It forms a beaded chain which connects both ends of the system and is similar to necklace states studied in [31].

2.4. Influence of other localized modes

To investigate how much different localized modes of the system contribute to the degenerate state $|\tilde{\Psi}_{\mathrm{EP}(1,2)}\rangle$, we measure their spatial overlap with the degenerate eigenstate. The norm of their biorthogonal projection, $|\langle\Psi_i^*|\tilde{\Psi}_{\mathrm{EP}(1,2)}\rangle|$, is shown in Fig. 3(a). Remarkably enough, it demonstrates the fading, though not negligible, influence of nearby modes with $i > 2$. Both modes 1 and 2 contribute to 60% to the degenerate EP state, while other modes have a vanishing contribution with increasing index, though modes 4 and 5, still contribute significantly for 25%. Their influence is also highlighted in Fig. 3(b), where the position of the EP, $(\Delta\epsilon_1, \Delta\epsilon_2)_{\mathrm{EP}}$, is calculated using the analytical prediction, Eq. (11), for an increasing number of contributing

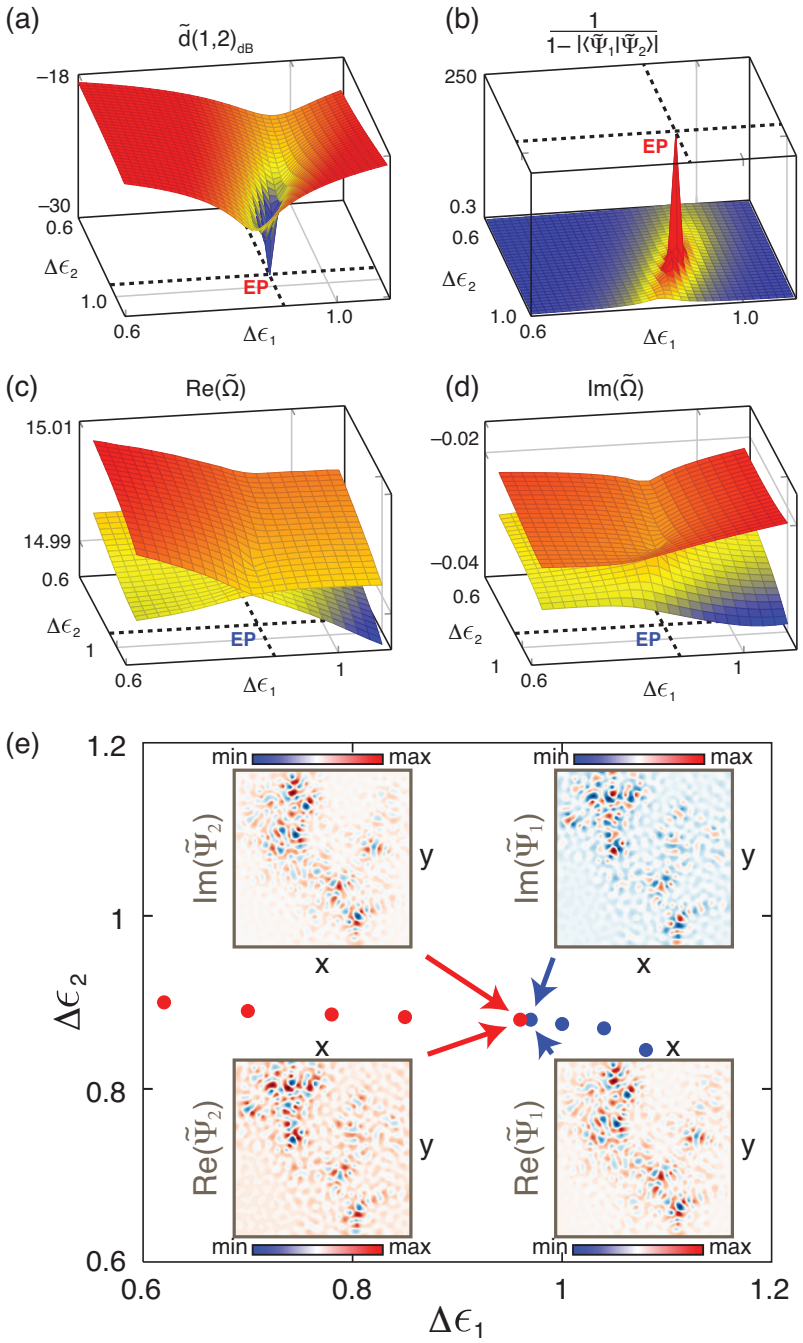

Fig. 2. (a) The eigenvalue difference $\tilde{d}(1,2)_{\mathrm{dB}} = |\tilde{\Omega}_1 - \tilde{\Omega}_2|_{\mathrm{dB}}$ (arbitrary units) vanishes at the position $(\Delta\epsilon_1, \Delta\epsilon_2)_{\mathrm{EP}}$ in parameter space. (b) The function $(1 - |\langle\tilde{\Psi}_1|\tilde{\Psi}_2\rangle|)^{-1}$ measures the collinearity of the eigenvectors and has a clear divergent maximum at $(\Delta\epsilon_1, \Delta\epsilon_2)_{\mathrm{EP}}$ where the two modes coalesce. (c) and (d) Real and imaginary part of the eigenvalues $\tilde{\Omega}_1$ and $\tilde{\Omega}_2$. The eigenvalue surfaces display the typical structure of intersecting Riemann sheets with a singular point at $(\Delta\epsilon_1, \Delta\epsilon_2)_{\mathrm{EP}}$. (e) Trajectories $\mathrm{Im}(\tilde{\Omega}_1) = \mathrm{Im}(\tilde{\Omega}_2)$ and $\mathrm{Re}(\tilde{\Omega}_1) = \mathrm{Re}(\tilde{\Omega}_2)$ marked by red and blue dots, respectively: Both curves join continuously at the EP. The insets show the real and imaginary part of modes 1 and 2 near the EP: the modes become collinear and satisfy $\tilde{\Psi}_1 = -i\tilde{\Psi}_2$ ($\mathrm{Re}(\tilde{\Psi}_1) = \mathrm{Im}(\tilde{\Psi}_2)$ and $\mathrm{Im}(\tilde{\Psi}_1) = -\mathrm{Re}(\tilde{\Psi}_2)$).

modes N. Fluctuations of the EP position are large for small N, while the convergence is reached for value of N larger than 55. This observation emphasizes a fundamental point, namely that the spatial amplitude distribution of the degenerate state at the EP results from the coupling of a large number of modes.

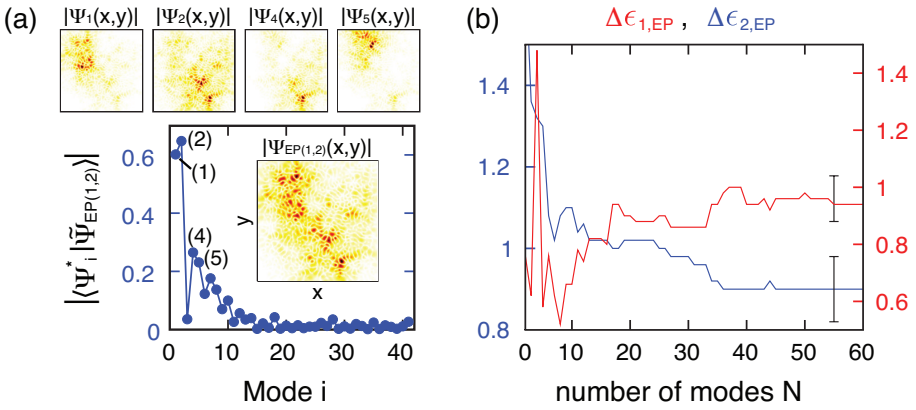

Fig. 3. (a) Norm of the biorthogonal projection of the degenerate eigenstate at the EP (coalescence of modes 1 and 2) with the first 45 initial modes $|\langle \Psi_i^* | \tilde{\Psi}_{\mathrm{EP}(1,2)} \rangle|$. The absolute value of the amplitude of $|\tilde{\Psi}_{\mathrm{EP}(1,2)}\rangle$ is shown in the inset. The four panels on top display the spatial distributions of initial modes 1, 2, 4 and 5, respectively. Their respective biorthogonal projection coefficient is numbered. (b) Prediction of EP position in the parameter space [$\Delta\epsilon_{1,\mathrm{EP}}$ (red line) and $\Delta\epsilon_{2,\mathrm{EP}}$ (blue line)] for a number of modes N, ranging from 2 to 60. The prediction converges for $N \geq 55$. The two error bars point out the position of the EP obtained by FEM computation.

3. Conclusion

In conclusion, we proposed a general analytical theory to study the evolution of modes in open media when the permittivity is varied. This non-perturbative approach relies on the linearity of $\epsilon(\mathbf{r})$ in the Helmholtz equation: For any variation ($\Delta\epsilon_1$, $\Delta\epsilon_2$) a new set of modes can be computed from Eq. (11) simply from the knowledge of the initial system. This approach describes the system by an infinite set of modes acting as oscillators coupled via the modification of the permittivity. We considered the specific case of random media in the localization regime and show that our theory can be used to investigate the mode coupling and hybridization resulting from a local perturbation. In particular, by changing the local index at two different small areas, two modes are brought to coalescence and give rise to an EP. Remarkably, the accuracy of the theoretical prediction is shown to strongly depend on the number of modes considered. A large number of initial modes is required, which shows that the mode evolution is dictated by multimode interactions. In terms of experimental realization, such a manipulation of the disorder can be easily implemented on existing setups [27, 52, 53]. The permittivity landscape can be shaped reversibly, e.g. using laser illumination to switch on a nonlinear Kerr index change. EPs can be calculated for any pair of modes and even generalized to hybridization of three or more eigenstates, which opens the way to the control of light-matter interaction in random media. The effective creation of necklace states, for instance, allows the formation of open transmission channels in opaque systems. Alternatively, using mode repulsion in the vicinity of an EP, the disorder can be engineered to increase the spatial confinement of the modes and consequently their Q-factor. Finally, we believe this approach can be extended to others types of complex optical systems, e.g. photonic crystal cavity arrays used for quantum simulation [42, 43, 54] where

fabrication inaccuracy could be compensated *a posteriori* by such an external control.

Funding. This research was supported by the Israel Science Foundation (Grants No. 1871/15, 2074/15 and 2630/20) and the United States-Israel Binational Science Foundation NSF/BSF (Grant No. 2015694). P. S. is also thankful to the Agence Nationale de la Recherche for its support under grant ANR PLATON (No. 12-BS09-003-01), the LABEX WIFI (Laboratory of Excellence within the French Program 'Investments for the Future') under reference ANR-10-IDEX-0001-02 PSL*, the CNRS support under grant PICS-ALAMO and the Groupement de Recherche 3219 MesoImage.

Acknowledgments. We thank S. Rotter for enlightening and fruitful discussions.

Disclosures. The authors declare no conflicts of interest.

Data Availability Statement. Data underlying the results presented in this paper are not publicly available at this time but may be obtained from the authors upon reasonable request.

References

1. W. D. Heiss and A. L. Sannino, "Avoided level crossing and exceptional points," J. Phys. A **23**, 1167–1178 (1990).
2. R. S. Whitney and Y. Gefen, "Berry Phase in a Nonisolated System," Phys. Rev. Lett. **90**, 190402 (2003).
3. A. Carollo, I. Fuentes-Guridi, M. F. Santos, and V. Vedral, "Geometric Phase in Open Systems," Phys. Rev. Lett. **90**, 160402 (2003).
4. T. Kato, *Perturbation theory for linear operators*, vol. 132 of *Classics in Mathematics* (Springer-Verlag Berlin Heidelberg, Berlin, Heidelberg, 1995), 2nd ed.
5. W. D. Heiss, "Phases of wave functions and level repulsion," Eur. Phys. J. D **7**, 1–4 (1999).
6. M. Liertzer, L. Ge, A. Cerjan, A. D. Stone, H. E. Türeci, and S. Rotter, "Pump-induced exceptional points in lasers," Phys. Rev. Lett. **108**, 173901 (2012).
7. J. Feilhauer, A. Schumer, J. Doppler, A. A. Mailybaev, J. Böhm, U. Kuhl, N. Moiseyev, and S. Rotter, "Encircling exceptional points as a non-Hermitian extension of rapid adiabatic passage," Phys. Rev. A **102**, 040201 (2020).
8. Y. Choi, S. Kang, S. Lim, W. Kim, J.-R. Kim, J.-H. Lee, and K. An, "Quasieigenstate Coalescence in an Atom-Cavity Quantum Composite," Phys. Rev. Lett. **104**, 153601 (2010).
9. M. Kammerer, F. Merz, and F. Jenko, "Exceptional points in linear gyrokinetics," Phys. Plasmas **15**, 052102 (2008).
10. W. D. Heiss and M. Müller, "Universal relationship between a quantum phase transition and instability points of classical systems," Phys. Rev. E **66**, 016217 (2002).
11. M. Brandstetter, M. Liertzer, C. Deutsch, P. Klang, J. Schöberl, H. E. Türeci, G. Strasser, K. Unterrainer, and S. Rotter, "Reversing the pump dependence of a laser at an exceptional point," Nat. Commun. **5**, 4034 (2014).
12. S. Klaiman, U. Günther, and N. Moiseyev, "Visualization of Branch Points in $\mathcal{PT}$-Symmetric Waveguides," Phys. Rev. Lett. **101**, 080402 (2008).
13. A. Guo, G. J. Salamo, D. Duchesne, R. Morandotti, M. Volatier-Ravat, V. Aimez, G. A. Siviloglou, and D. N. Christodoulides, "Observation of $\mathcal{PT}$-Symmetry Breaking in Complex Optical Potentials," Phys. Rev. Lett. **103**, 093902 (2009).
14. M. P. Hokmabadi, A. Schumer, D. N. Christodoulides, and M. Khajavikhan, "Non-Hermitian ring laser gyroscopes with enhanced Sagnac sensitivity," Nature **576**, 70–74 (2019).
15. Y.-H. Lai, Y.-K. Lu, M.-G. Suh, Z. Yuan, and K. Vahala, "Observation of the exceptional-point-enhanced Sagnac effect," Nature **576**, 65–69 (2019).
16. C. Wang, W. R. Sweeney, A. D. Stone, and L. Yang, "Coherent perfect absorption at an exceptional point," Science **373**, 1261–1265 (2021).
17. B. Dietz, H. L. Harney, O. N. Kirillov, M. Miski-Oglu, A. Richter, and F. Schäfer, "Exceptional Points in a Microwave Billiard with Time-Reversal Invariance Violation," Phys. Rev. Lett. **106**, 150403 (2011).
18. S.-B. Lee, J. Yang, S. Moon, S.-Y. Lee, J.-B. Shim, S. W. Kim, J.-H. Lee, and K. An, "Observation of an Exceptional Point in a Chaotic Optical Microcavity," Phys. Rev. Lett. **103**, 134101 (2009).
19. H. Xu, D. Mason, L. Jiang, and J. G. E. Harris, "Topological energy transfer in an optomechanical system with exceptional points," Nature **537**, 80–83 (2016).
20. Y. Zhu and L. Zhu, "Accessing the Exceptional Points in Coupled Fabry–Perot Resonators through Hybrid Integration," ACS Photonics **5**, 4920–4927 (2018).
21. K. H. Kim, M. S. Hwang, H. R. Kim, J. H. Choi, Y. S. No, and H. G. Park, "Direct observation of exceptional points in coupled photonic-crystal lasers with asymmetric optical gains," Nat. Commun. **7**, 13893 (2016).
22. K. Ding, G. Ma, M. Xiao, Z. Q. Zhang, and C. T. Chan, "Emergence, Coalescence, and Topological Properties of Multiple Exceptional Points and Their Experimental Realization," Phys. Rev. X **6**, 021007 (2016).
23. A. Bergman, R. Duggan, K. Sharma, M. Tur, A. Zadok, and A. Alù, "Observation of anti-parity-time-symmetry, phase transitions and exceptional points in an optical fibre," Nat. Commun. **12**, 486 (2021).
24. Y. Choi, C. Hahn, J. W. Yoon, and S. H. Song, "Observation of an anti-PT-symmetric exceptional point and energy-difference conserving dynamics in electrical circuit resonators," Nat. Commun. **9**, 1–6 (2018).
25. P. W. Anderson, "Absence of Diffusion in Certain Random Lattices," Phys. Rev. **109**, 1492–1505 (1958).

26. V. Milner and A. Z. Genack, "Photon Localization Laser: Low-Threshold Lasing in a Random Amplifying Layered Medium via Wave Localization," Phys. Rev. Lett. **94**, 073901 (2005).
27. J.-K. Yang, H. Noh, M. J. Rooks, G. S. Solomon, F. Vollmer, and H. Cao, "Lasing in localized modes of a slow light photonic crystal waveguide," Appl. Phys. Lett. **98**, 241107 (2011).
28. B. Kumar, R. Homri, Priyanka, S. K. Maurya, M. Lebental, and P. Sebbah, "Localized modes revealed in random lasers," Optica **8**, 1033–1039 (2021).
29. L. Sapienza, H. Thyrrestrup, S. Stobbe, P. D. Garcia, S. Smolka, and P. Lodahl, "Cavity quantum electrodynamics with anderson-localized modes," Science **327**, 1352–1355 (2010).
30. J. Gao, S. Combrie, B. Liang, P. Schmitteckert, G. Lehoucq, S. Xavier, X. Xu, K. Busch, D. L. Huffaker, A. De Rossi, and C. W. Wong, "Strongly coupled slow-light polaritons in one-dimensional disordered localized states," Sci. Reports **3**, 1–6 (2013).
31. L. Labonté, C. Vanneste, and P. Sebbah, "Localized mode hybridization by fine tuning of two-dimensional random media," Opt. Lett. **37**, 1946–1948 (2012).
32. J. Bertolotti, S. Gottardo, D. S. Wiersma, M. Ghulinyan, and L. Pavesi, "Optical Necklace States in Anderson Localized 1D Systems," Phys. Rev. Lett. **94**, 113903 (2005).
33. P. Sebbah, B. Hu, J. M. Klosner, and A. Z. Genack, "Extended Quasimodes within Nominally Localized Random Waveguides," Phys. Rev. Lett. **96**, 183902 (2006).
34. J. B. Pendry, "Quasi-extended electron states in strongly disordered systems," J. Phys. C: Solid State Phys. **20**, 733 (1987).
35. J. B. Pendry, "Symmetry and transport of waves in one-dimensional disordered systems," Adv. Phys. **43**, 461–542 (1994).
36. C. Vanneste and P. Sebbah, "Complexity of two-dimensional quasimodes at the transition from weak scattering to Anderson localization," Phys. Rev. A **79**, 041802 (2009).
37. A. F. Tzortzakakis, K. G. Makris, and E. N. Economou, "Non-Hermitian disorder in two-dimensional optical lattices," Phys. Rev. B **101**, 014202 (2020).
38. S. Kalish, Z. Lin, and T. Kottos, "Light transport in random media with PT symmetry," Phys. Rev. A - At. Mol. Opt. Phys. **85**, 055802 (2012).
39. O. Bendix, R. Fleischmann, T. Kottos, and B. Shapiro, "Exponentially Fragile $\mathcal{PT}$ Symmetry in Lattices with Localized Eigenmodes," Phys. Rev. Lett. **103**, 030402 (2009).
40. H. Vemuri, V. Vavilala, T. Bhamidipati, and Y. N. Joglekar, "Dynamics, disorder effects, and $\mathcal{PT}$-symmetry breaking in waveguide lattices with localized eigenstates," Phys. Rev. A **84**, 043826 (2011).
41. O. Vázquez-Candanedo, J. C. Hernández-Herrejón, F. M. Izrailev, and D. N. Christodoulides, "Gain- or loss-induced localization in one-dimensional $\mathcal{PT}$-symmetric tight-binding models," Phys. Rev. A **89**, 013832 (2014).
42. M. J. Hartmann, F. G. S. L. Brandão, and M. B. Plenio, "Strongly interacting polaritons in coupled arrays of cavities," Nat. Phys. **2**, 849–855 (2006).
43. A. D. Greentree, C. Tahan, J. H. Cole, and L. C. L. Hollenberg, "Quantum phase transitions of light," Nat. Phys. **2**, 856–861 (2006).
44. P. T. Leung, S. Y. Liu, S. S. Tong, and K. Young, "Time-independent perturbation theory for quasinormal modes in leaky optical cavities," Phys. Rev. A **49**, 3068–3073 (1994).
45. P. T. Leung, S. Y. Liu, and K. Young, "Completeness and orthogonality of quasinormal modes in leaky optical cavities," Phys. Rev. A **49**, 3057–3067 (1994).
46. P. T. Leung, W. M. Suen, C. P. Sun, and K. Young, "Waves in open systems via a biorthogonal basis," Phys. Rev. E **57**, 6101–6104 (1998).
47. P. M. Morse and H. Feshbach, *Methods of theoretical physics* (McGraw-Hill, New York, 1953).
48. N. Moiseyev, P. R. Certain, and F. Weinhold, "Resonance properties of complex-rotated hamiltonians," Mol. Phys. **36**, 1613–1630 (1978).
49. R. Touzani, "OFELI, An Object Oriented Finite Element Library," (2013).
50. V. Hernandez, J. E. Roman, and V. Vidal, "SLEPc: A Scalable and Flexible Toolkit for the Solution of Eigenvalue Problems," ACM Transactions on Math. Softw. **31**, 351–362 (2005).
51. M. B. Doost, W. Langbein, and E. A. Muljarov, "Resonant state expansion applied to two-dimensional open optical systems," Phys. Rev. A **87**, 043827 (2013).
52. F. Riboli, P. Barthelemy, S. Vignolini, F. Intonti, A. De Rossi, S. Combrie, and D. S. Wiersma, "Anderson localization of near-visible light in two dimensions," Opt. Lett. **36**, 127–129 (2011).
53. F. Riboli, N. Caselli, S. Vignolini, F. Intonti, K. Vynck, P. Barthelemy, A. Gerardino, L. Balet, L. H. Li, A. Fiore, M. Gurioli, and D. S. Wiersma, "Engineering of light confinement in strongly scattering disordered media," Nat. Mater. **13**, 720–725 (2014).
54. A. Majumdar, A. Rundquist, M. Bajcsy, V. D. Dasika, S. R. Bank, and J. Vučković, "Design and analysis of photonic crystal coupled cavity arrays for quantum simulation," Phys. Rev. B **86**, 195312 (2012).